Journal of Materials Chemistry A

RSC Publishing

COMMUNICATION

View Article Online
View Journal | View Issue

Cite this: *J. Mater. Chem. A*, 2013, **1**, 3860

Received 22nd December 2012
Accepted 6th February 2013

DOI: 10.1039/c3ta01618h

www.rsc.org/MaterialsA

Synthesis of single crystalline hexagonal nanobricks of $LiNi_{1/3}Co_{1/3}Mn_{1/3}O_2$ with high percentage of exposed {010} active facets as high rate performance cathode material for lithium-ion battery†

Fang Fu, Gui-Liang Xu, Qi Wang, Ya-Ping Deng, Xue Li, Jun-Tao Li, Ling Huang and Shi-Gang Sun*

Single crystalline $LiNi_{1/3}Co_{1/3}Mn_{1/3}O_2$ (LNCM) hexagonal nanobricks with a high percentage of exposed {010} facets are synthesized by using $Ni_{1/3}Co_{1/3}Mn_{1/3}(OH)_2$ hexagonal nanosheets as both template and precursor, and exhibit excellent high rate performance as a cathode of lithium ion batteries.

Lithium-ion batteries (LIBs) have played an important role in portable electronics, and they are intensively pursued as a power source for vehicle applications.[1,2] However, the presently available cathodes with limited capacity could not meet the high energy requirements of practical applications, and there is therefore immense interest in developing cathode materials. Layer-structured $LiNi_{1/3}Co_{1/3}Mn_{1/3}O_2$ (LNCM), owing to its high theoretical capacity (278 mA h g^{-1}), structural stability and thermal stability, is regarded as one of the most promising alternative cathode materials in the past decades.[3–6] Nevertheless, the sluggish diffusion of electrons and lithium ions within $LiNi_{1/3}Co_{1/3}Mn_{1/3}O_2$ results in a rapidly fading capacity and inferior rate capability.[7,8] To solve these problems and improve the electrochemical performances of LNCM materials, many attempts, such as surface coating[9–11] and fabricating nanoparticles[12,13] have been conducted. However, the surface coating tends to lower the overall capacity, and the high specific surface area of nanomaterials could cause undesirable side reactions. As a consequence, these strategies can only improve the performance to a certain extent.[14,15] Since the properties depend strongly on the structure of nanomaterials, to design and control rationally the structure and morphology of LNCM nanomaterials presents an effective route to enhance the capacity retention and rate performance.

LNCM hexagonal crystallites possess a layer-structure with the $R\bar{3}m$ space group, as shown in Fig. S1 in ESI.† The structure is made up of MO_2 oxygen layers perpendicular to the *c* axis,[16–18] indexed as {001} planes that include the (001) and (00$\bar{1}$) facets at the top and bottom, respectively of the hexagonal crystal. The {001} planes are formed by NiO_6, CoO_6 and MnO_6 octahedra, which interconnect to each other by corner-sharing oxygen atoms, and consist of a close-packed structure that hinders Li^+ insertion along the *c* axis. The close packed {001} planes are therefore not electrochemically active for Li^+ transportation. The 6-sided facets of the hexagonal crystal, *i.e.* (010), (0$\bar{1}$0), (100), (110), (1$\bar{1}$0) and ($\bar{1}$00) facets, are denoted as {010} facets, which are perpendicular to the {001} planes and have an open structure with a wide window between the layers for Li^+ migration. This structural analysis indicates that Li^+ transport in LNCM is two-dimensional parallel to the Li^+ layers along the *a* (or *b*) axis. Due to the low surface energy of the {001} planes, LNCM nanomaterials are normally exposed mainly with {001} facets. Therefore, to promote the growth of the LNCM crystal along the *c*-direction and inhibit the growth along the *a* and *b* directions will produce LNCM crystals with a high percentage of exposed {010} facets which could facilitate the fast and efficient transportation of Li^+, and achieve superior electrochemical performance. In our previous studies, we have demonstrated that lithium Mn-rich metal oxides with a high percentage of exposed {010} facets exhibit superior rate-performance.[19]

Although the directed particle growth can be manipulated with the aid of hard or soft templates, it is very difficult to grow LNCM along the *c* direction owing to its intrinsic lamellar structure and the high surface energy of the {010} planes.[19] As the crystal growth rate of a high-energy plane is faster than that of a low-energy plane, the high-energy planes have a tendency to disappear during growth, and the surface of the resulting crystal will be dominated by low-energy planes.[20] To the best of our knowledge, well-defined LNCM nanocrystals with a high percentage of {010} facets have never been reported yet. As a consequence, it remains a big challenge to synthesize single-crystalline LNCM with controlled crystal size along the *c* direction.

State Key Laboratory of Physical Chemistry of Solid Surfaces, Department of Chemistry, College of Chemistry and Chemical Engineering, School of Energy Research, Xiamen University, Xiamen 361005, China. E-mail: sgsun@xmu.edu.cn

† Electronic supplementary information (ESI) available: Experimental details, schematic model, particle size distribution, XRD/SEM/TEM data, as well as electrochemical data. See DOI: 10.1039/c3ta01618h

In the present paper, we present a precursor–template method for the synthesis of LNCM hexagonal nanobricks that have a percentage of exposed {010} facets as high as *ca.* 58.6%, and exhibit excellent high rate performance as a cathode of lithium ion batteries.

The main process of synthesizing the LNCM nanobricks is illustrated in Fig. 1, in which the $Ni_{1/3}Co_{1/3}Mn_{1/3}(OH)_2$ hexagonal nanosheets served as both template and precursor. The synthesis can be approximately divided into two stages: (1) adsorbate-directed synthesis of the $Ni_{1/3}Co_{1/3}Mn_{1/3}(OH)_2$ precursor, and (2) growth of $Ni_{1/3}Co_{1/3}Mn_{1/3}(OH)_2$ template crystals into nanobricks. In the adsorbate-directed synthesis of the precursor, the surface-capping agent poly(vinylpyrrolidone) (PVP) plays a crucial role in the formation of a plate-like $Ni_{1/3}Co_{1/3}Mn_{1/3}(OH)_2$ structure. The addition of a relatively large amount of PVP into the reaction solution causes a quite viscous environment, allowing slow nucleation of the precursor.[21] Soon after the plate-like structure is formed, PVP molecules immediately adsorb on its negatively charged {001} surfaces *via* the amine groups,[22,23] thus reducing the growth rate along the [001] direction and leading to the formation of (001)-plane-dominated nanoplates (Fig. S2 in ESI†). These nanoplates are about 50–200 nm in edge length and 10 nm in thickness. The crystal structure of the precursor was identified by powder X-ray diffraction (XRD), as shown in Fig. S3 in ESI.† The main peaks of the XRD pattern can be indexed as hydroxide phases, which are the most probable structures that can form during co-precipitation. A small amount of Mn_3O_4 spinel could also be observed in the XRD pattern and this is inevitable, because Mn^{2+} can be easily oxidized.[24,25] Then the produced precursor $Ni_{1/3}Co_{1/3}Mn_{1/3}(OH)_2$ mixed with lithium is calcined at high temperature. After heat treatment at 450 °C, the polymer PVP is decomposed and a few lithium ions have inserted into the precursor (Fig. S4 in ESI†). With increasing calcination temperature, the mass mobility quickens and the high mobility Li^+ continues to insert into the space between the layers of $Ni_{1/3}Co_{1/3}Mn_{1/3}(OH)_2$ along the [001] direction, accompanied by the formation of LNCM nuclei on its surface.[26] When the calcination temperature is higher than 800 °C but does not exceed 1000 °C, the parent crystals, *i.e.* the $Ni_{1/3}Co_{1/3}Mn_{1/3}(OH)_2$ hexagonal nanosheets with the insertion of Li^+ along the [010] direction, are converted completely into LNCM nanobricks and resulted in a significant increase in the percentage of lateral {010} facets. The atomic arrangements of the {001} and {010} planes clearly reveal that the close packed {001} planes are unfavorable for Li^+ transportation, and the open {010} planes with many channels along the *a* or *b* directions are active planes for Li^+ transportation.

When annealing at a relatively low temperature such as 450 °C, the obtained products exhibit nanoplate morphology with sidewall thickness of only around 21.7 nm (Fig. S5a in ESI†). It is worth pointing out that the ratio (*H*/*L*) of the sidewall thickness (*H*) over the edge length (*L*) of the nanobrick is a direct reflection of the percentage of {010} facets on the surface of nanobrick. We found that with increasing annealing temperature, the *H* of the nanocrystals gradually increases, while the edge length (*L*) changes very little, resulting in an increase in *H*/*L*. When the annealing temperatures are at respectively 800 and 900 °C, the sidewall thicknesses of the nanobricks are correspondingly measured as 67.2 and 141.7 nm (Fig. S5b and c, S6 and S7 in ESI†), and the *H*/*L* is proportionally increased from 0.365 to 0.709. At the same time, the proportion of the active surface area, that is, the surface area of {010} facets over the total surface area of the nanobricks is increased from 42.2% to 58.6%.

We found that the calcination temperature could not be too high; otherwise the LNCM crystalline structure would be changed. When calcined at 1000 °C, the layered structure has been transformed into a spinel structure, as shown in Fig. S5d (ESI†). The above results indicate that an appropriate calcination temperature is the engine that drives the crystal growth along the [001] direction, and 900 °C is found to be the preferred temperature for the growth of {010} planes. With more active {010} planes formed at 900 °C, the character of the LNCM nanobricks prepared at this annealing temperature is systematically investigated thereafter.

Fig. 2a and b show the scanning electron microscopy (SEM) images of the as-prepared LNCM sample. We observe clearly that the sample consists of nanobricks of well-defined hexagonal shape with smooth surface and extended sidewalls. The insets to Fig. 2a and b illustrate clear views of the LNCM nanobricks, which further confirm that they have a perfect hexagonal shape with sharp corners and edges. The crystal structure of the LNCM nanobricks was studied by XRD. All reflections in the XRD patterns (Fig. 2c) can be indexed as the α-$NaFeO_2$ phase. The peak intensity ratio $I(003)/I(104)$ (equal to 2.07) and the clear splitting of (006)/(012) and (108)/(110) doublets suggest the well-ordered layer-structure of the prepared LNCM.[27–29]

The transmission electron microscopy (TEM) characterization of the LCNM nanobricks is displayed in Fig. 3. Well-defined hexagonal nanobricks with thick sidewalls can be seen from the images in Fig. 3a and c, which are in good agreement with the above SEM findings. The HR-TEM image (Fig. 3b) of the frontal plane displays two sets of clear lattice fringes with the same interplanar distance of 0.246 nm at an angle of 120°, corresponding to the $(0\bar{1}0)$ and (100) planes of LNCM, respectively. These observations indicate that the frontal plane of the

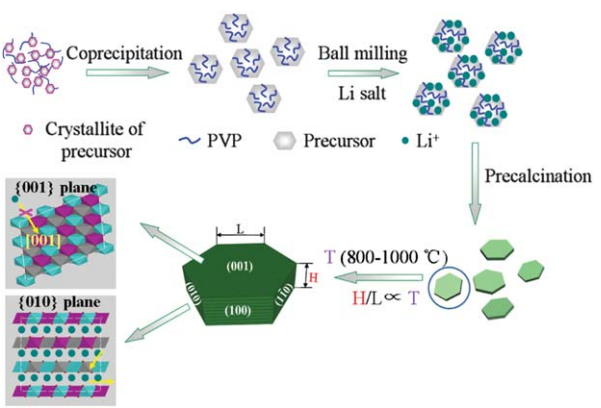

Fig. 1 Schematic illustration of the formation of LNCM nanobricks by a precursor–template process.

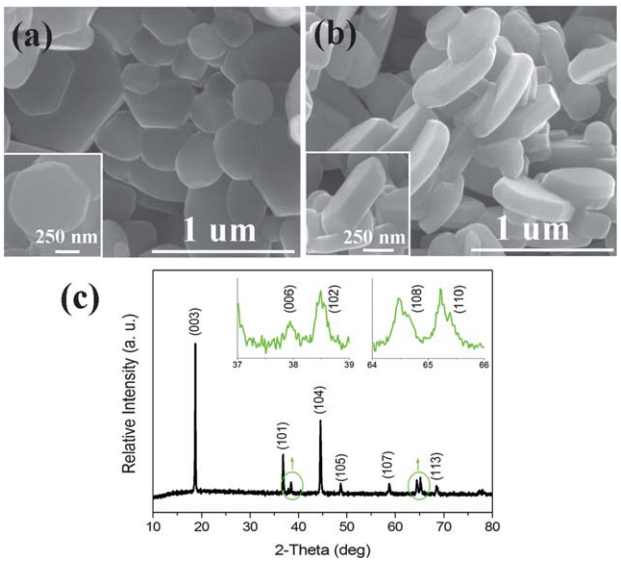

Fig. 2 (a) SEM image of the frontal view of LNCM nanobricks and a magnified image of a single nanobrick. (b) SEM image of the lateral view of LNCM nanobricks and a magnified image of a single nanobrick. (c) XRD pattern of LNCM nanobricks.

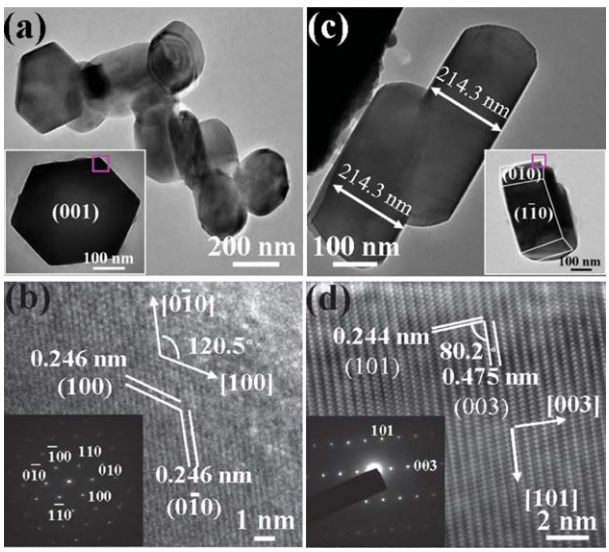

Fig. 3 (a) TEM images of the frontal view of LNCM nanobricks and a magnified image of a single nanobrick. (b) HRTEM image and SAED pattern of the frontal plane of a single nanobrick shown in (a). (c) TEM images of the lateral view of LNCM nanobricks and a magnified image of a single nanobrick. (d) HRTEM image and SAED pattern of the lateral plane of a single nanobrick shown in (c).

nanobricks is the (001) plane. The corresponding selected area electron diffraction (SAED) pattern (Fig. 3b, inset) showing an array of hexagonal symmetry dots proves that these nanobricks are single-crystalline, and have a hexagonal structure capped by a (001) plane. Fig. 3d depicts lattice fringes of one lateral plane with spacings of 0.475 and 0.244 nm, respectively. Such values coincide with the interplanar distances of the (003) and (101) planes of LNCM, and confirm that this lateral plane is the (0$\bar{1}$0) plane. The other five lateral planes are (010), ($\bar{1}$00), (1$\bar{1}$0), (110) and (100), which can be inferred according to the hexagonal structure of the LNCM. These {010} lateral planes parallel to the *c* axis are normal to the facile pathway for lithium ion migration, and hence electrochemically active. Moreover, from the HR-TEM results, it is worth noting that the (001) planes possess dense atom arrangements, whereas the (0$\bar{1}$0) planes have relatively loose packing, especially along the [001] direction, which consequently has large channels along the [001] direction. Such character reflects the openness of the structure. These results are in good agreement with the simulated crystal structure of LNCM (Fig. S1 in ESI†), and experimentally confirm that Li^+ can only intercalate/deintercalate through the tunnels perpendicular to the [001] direction. The increased thickness of the nanobricks in the [001] direction provides more channels for lithium ion migration, and consequently enhances the electrochemical performance of the LNCM.

The electrochemical performances of the LNCM nanobricks at higher rates are shown in Fig. 4. The initial charge and discharge capacities at a rate of 1 C (Fig. S8a, ESI†) are measured as 208.6 mA h g^{-1} and 179.2 mA h g^{-1}, respectively. The discharge capacity at 1 C demonstrates no significant loss in the first twenty cycles, and is 165.3 mA h g^{-1} after 50 cycles, which corresponds to 90.6% capacity retention (Fig. S8b, ESI†). As shown in Fig. 4, the initial discharge capacities are measured as 159.1, 151.3, 136.1 and 130 mA h g^{-1}, corresponding to 2, 5, 10 and 15 C rates, respectively. These specific discharge capacities at high rates are superior to those of the highest values reported so far for LNCM materials in the literature.[30–35] It is found that along with the increase in cycle number, the discharge capacity is increasing within a few initial cycles, and then reaches its maximum. Such a phenomenon is known as the activation of the cell at higher current density of charge/discharge. So we take the maximum values of the discharge capacity to calculate the capacity retention. The capacity retentions of the LNCM nanobricks at 2 C, 5 C, 10 C and 15 C rates after 100 cycles are then calculated as 89%, 91.2%, 93.5%

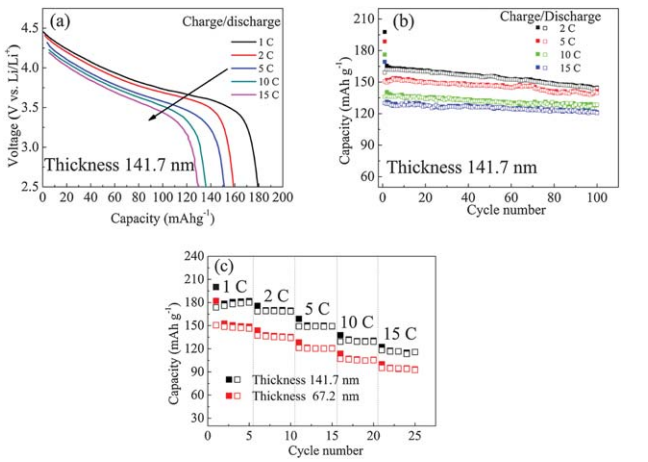

Fig. 4 (a) First discharge profiles of LNCM cycled at different rates in the voltage range between 2.5 and 4.6 V. (b) Cycling performance of LNCM at high rates. (c) Comparison of the rate capability of the nanobricks with different sidewall thickness.

and 91.9%, respectively. These results demonstrate that the as-synthesized LNCM nanobricks exhibit intrinsically excellent cyclic stability at high rate. This high rate performance would be beneficial for meeting the high-power requirement for the next generation of lithium ion batteries. The excellent cycling performance of the nanobricks at high rate can be ascribed to their high-quality crystallinity and relatively perfect hexagonal shape with a high percentage of exposed {010} facets. The high crystallinity of the nanobricks can improve the stability of the crystallographic structure of LNCM upon cycling.[36,37] More importantly, the relatively perfect hexagonal shape with a high percentage of exposed {010} facets of the LNCM ensures an ordered atomic arrangement, which facilitates the Li ion diffusion inside the crystal.

To investigate the effect of the {010} plane on the electrochemical performance of LNCM nanobricks, the discharge capacity of nanobricks with sidewall thicknesses of 141.7 and 67.2 nm at different rates (1 C, 2 C, 5 C, 10 C and 15 C) are compared in Fig. 4c. At all rates tested, the nanobricks with a thickness around 141.7 nm always deliver a higher capacity than that of the nanobricks with a thickness around 67.2 nm. The capacity difference between the two samples at different rates is around 30 mA h g^{-1}. This result confirms that the nanobricks of thickness around 141.7 nm with a higher percentage of exposed {010} facets lead to higher discharge capacity and better rate performance. The excellent electrochemical performance of the nanobricks with higher thickness could be attributed to their unique hexagonal brick structure, which provides a high percentage of exposed {010} planes along the [001] direction and results in more channels for fast and efficient lithium intercalation/deintercalation.

In summary, single-crystal LNCM hexagonal nanobricks with significantly increased sidewall thickness along the [001] direction are synthesized by a precursor–template method. When serving as cathode materials of lithium ion batteries, the as-synthesized LNCM nanobricks with a thickness around 141.7 nm demonstrate excellent cyclic stability at high rate, which is attributed to their unique nanostructures with a high percentage of exposed {010} facets along the [001] direction, which ensure fast and efficient lithium intercalation and deintercalation. This result is of significance in the rational design and synthesis of layer-structure LNCM cathode materials with high discharge capacity and excellent rate performance by increasing the exposed {010} active facets.

This work was supported by the Special Funds for Major State Basic Research Project of China (2009CB220102), "863" program (2011AA11A254) and a grant from NSFC (21021002).

Notes and references

1 P. Gibot, M. Casas-Cabanasb, L. Laffont, S. Levasseur, P. Carlach, S. Hamelet, J. M. Tarascon and C. Masquelier, *Nat. Mater.*, 2008, **7**, 741.
2 J. M. Tarascon and M. Armand, *Nature*, 2001, **414**, 359.
3 Y. K. Sun, S. T. Myung, B. C. Park, J. Prakash, I. Belharouak and K. Amine, *Nat. Mater.*, 2009, **8**, 320.
4 K. M. Shaju and P. G. Bruce, *Adv. Mater.*, 2006, **18**, 2330.
5 N. Yabuuchi and T. Ohzuku, *J. Power Sources*, 2003, **171**, 119.
6 J. B. Goodenough and Y. Kim, *Chem. Mater.*, 2010, **22**, 587.
7 C. V. Rao, A. L. M. Reddy, Y. Ishikawa and P. M. Ajayan, *ACS Appl. Mater. Interfaces*, 2011, **3**, 2966.
8 C. M. Ban, Z. li, Z. C. Wu, M. J. Kirkham, L. Chen, Y. S. Jung, E. A. Payzant, Y. F. Yan, M. S. Whittingham and A. C. Dillon, *Adv. Energy Mater.*, 2011, **1**, 58.
9 J. T. Son and E. J. Cairns, *J. Power Sources*, 2007, **166**, 343.
10 S. H. Yun, K. S. Park and Y. J. Park, *J. Power Sources*, 2010, **195**, 6108.
11 J. Cho, Y. W. Kim, B. Kim, J. G. Lee and B. Park, *Angew. Chem., Int. Ed.*, 2003, **42**, 1618.
12 Z. D. Huang, X. M. Liu, S. W. Oh, B. Zhang, P. C. Ma and J. K. Kim, *J. Mater. Chem.*, 2011, **21**, 10777.
13 J. Jamnik and J. Maier, *Phys. Chem. Chem. Phys.*, 2003, **5**, 5215.
14 A. S. Arico, P. Bruce, B. Scrosati, J. M. Tarascon and W. Van Schalkwijk, *Nat. Mater.*, 2005, **4**, 366.
15 M. Okubo, J. Kim, T. Kudo, H. Zhou and I. Honma, *J. Phys. Chem. C*, 2009, **113**, 15337.
16 N. Igawa, T. Taguchi, H. Fukazawa, H. Yamauchi and W. Utsumi, *J. Am. Ceram. Soc.*, 2010, **8**, 2144.
17 N. Balke, S. Jesse, A. N. Morozovska, E. Eliseev, D. W. Chung, Y. Kim, L. Adamczyk, R. E. Gar, N. Dudney and S. V. Kalinin, *Nat. Nanotechnol.*, 2010, **5**, 749.
18 S. C. Yin, Y. H. Rho, I. Swainson and L. F. Nazar, *Chem. Mater.*, 2006, **18**, 1901.
19 G. Z. Wei, X. Lu, F. S. Ke, L. Huang, J. T. Li, Z. X. Wang, Z. Y. Zhou and S. G. Sun, *Adv. Mater.*, 2010, **22**, 4364.
20 M. Leng, M. Z. Liu, Y. B. Zhang, Z. Q. Wang, C. Yu, X. G. Yang, H. G. Zhang and C. Wang, *J. Am. Chem. Soc.*, 2010, **132**, 17084.
21 X. W. Lou, D. Deng, J. Y. Lee, J. Feng and L. A. Archer, *Adv. Mater.*, 2008, **20**, 258.
22 M. G. Kim, M. K. Jo, Y. S. Hong and J. Cho, *Chem. Commun.*, 2009, 218.
23 Y. H. Min, G. D. Moon, B. S. Kim, B. K. Lim, J. S. Kim, C. Y. Kang and U. Y. Jeong, *J. Am. Chem. Soc.*, 2012, **134**, 2872.
24 F. Zhou, X. M. Zhao, A. Van Bommel, A. W. Rowe and J. R. Dahn, *Chem. Mater.*, 2010, **22**, 1015.
25 A. W. Rowe and J. R. Dahn, *J. Electrochem. Soc.*, 2009, **156**, A362.
26 H. L. Chen, L. J. Wu, L. H. Zhang, Y. M. Zhu and C. P. Grey, *J. Am. Chem. Soc.*, 2011, **133**, 262.
27 B. J. Hwang, Y. W. Tsai, D. Carlier and G. Ceder, *Chem. Mater.*, 2003, **15**, 3676.
28 J. K. Ngala, N. A. Chernova, M. M. Ma, M. Mamak, P. Y. Zavalij and M. S. Whittingham, *J. Mater. Chem.*, 2004, **14**, 214.
29 Z. Li, F. Du, X. F. Bie, D. Zhang, Y. M. Cai, X. R. Cui, C. Wang, Z. G. Chen and Y. J. Wei, *J. Phys. Chem. C*, 2010, **114**, 22751.
30 S. H. Yun, K. S. Park and Y. J. Park, *J. Power Sources*, 2010, **195**, 6108.
31 J. T. Xu, S. L. Chou, Q. F. Gu, H. K. Liu and S. X. Dou, *J. Power Sources*, 2013, **225**, 172.

32 L. Q. Wang, L. F. Jiao, H. T. Yuan, J. Guo, M. Zhao, H. X. Li and Y. M. Wang, *J. Power Sources*, 2006, **162**, 1367.
33 T. Mei, Y. C. Zhu, K. B. Tang and Y. T. Qian, *RSC Adv.*, 2012, **2**, 12886.
34 X. Y. Han, Q. F. Meng, T. L. Sun and J. T. Sun, *J. Power Sources*, 2010, **195**, 3047.
35 D. C. Li, Y. K. Sasaki, K. Kobayakawa, H. Noguchi and Y. C. Sato, *Electrochim. Acta*, 2006, **52**, 643.
36 L. Z. Zhang, J. C. Yu, Q. Xu, K. Li, W. Kwong and L. Wu, *Chem. Commun.*, 2003, 2910.
37 Y. L. Ding, J. Xie, G. S. Cao, T. J. Zhu, H. M. Yu and X. B. Zhao, *Adv. Funct. Mater.*, 2011, **21**, 348.

